

Development of An Innovative Space Boom

Michael C. Lou and Houfei Fang
Jet Propulsion Laboratory
California Institute of California, Pasadena, California

Ben Yang and Nathaniel Lee Palmer
Department of Mechanical Engineering
University of Southern California, Los Angeles, California

Abstract

This paper presents the development of a new type of ultra-lightweight space boom, called the Self-deployable Spring Strip Boom or simply the S³ Boom. It describes the fundamental design concept and several variations of design configurations. Test results of proof-of-concept models are discussed and compared with results obtained by analytical simulations.

1.0 Introduction

Deployable booms of various designs form an important class of space structures. Booms deployed by mechanical means have long been employed to deploy solar arrays, antennas, sunshields, and various science instruments such as magnetometers and cameras. The use of deployable booms has become so common that at least one was incorporated in every flight system flown in the past. In fact, many space missions were enabled by the innovative use of deployable booms. For examples, short booms with deployed lengths of less than a couple of meters were used on the Mars Pathfinder to deploy an imager (Figure 1) and on the Mars Global Surveyor (Figure 2) to deploy a X-band high-gain relay antenna. Longer booms, which have extended lengths of several meters, were incorporated in the interplanetary spacecraft of Voyager (Figure 3) and the Galileo (Figure 4) to deploy magnetometers and other scientific sensors that need to be located far away from the spacecraft bus for accurate measurements. The recently flown Shuttle Radar Topography Mission (SRTM) also involved a highly innovative application of a 60-meter-long deployable space boom.

The objective of the SRTM, launched in early 2000 for a ten-day LEO mission, is to obtain elevation radar data on a near-global scale and generate the most complete high-resolution digital topographic database of the Earth. To achieve this goal, the

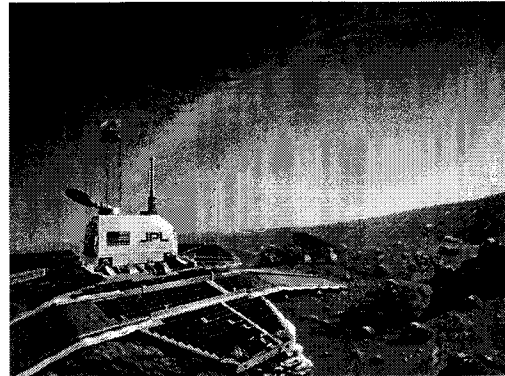


Figure 1. Mars Pathfinder Lander

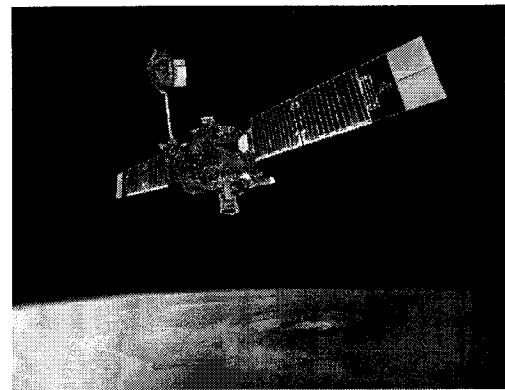


Figure 2 Mars Global Surveyor

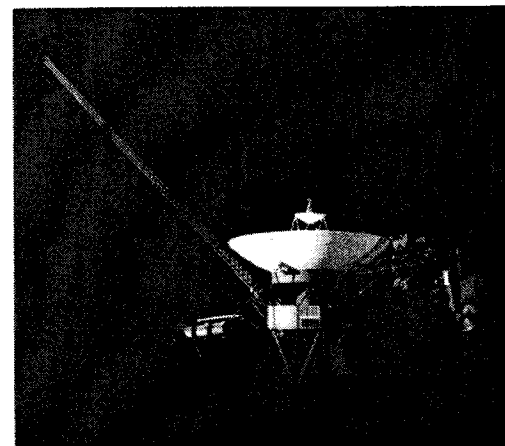


Figure 3. The Voyager Spacecraft

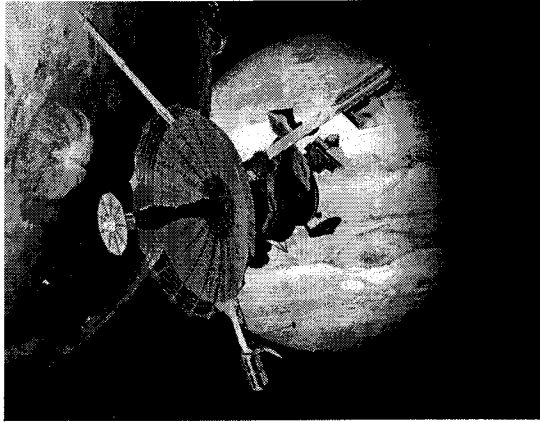


Figure 4. The Galileo Spacecraft

SRTM made use of radar interferometry. Two radar images are taken from different vantagepoints. Differences between these images allow for the calculation of surface elevation. The SRTM flight system payload was outfitted with two radar antennas. One antenna was located in the Shuttle's payload bay, the other, called the outboard antenna, is attached at the end of a 60-meter-long deployable boom that extended from the Shuttle's payload bay once the Shuttle was in space (see Figure 5). The boom, known as the SRTM mast, was the largest rigid structure ever flown in space and provided for the SRTM mission the baseline distance between the main antenna and the outboard antenna. This boom, was an Able Deployable Articulated Mast (ADAM) built by the AEC-Able Engineering Company. It was basically a truss structure that consists of 87 cube-shaped sections. Unique latches on the diagonal members of the truss allowed the mechanism to deploy section-by-section out of the containing canister to its fully extended length of 60 meters.

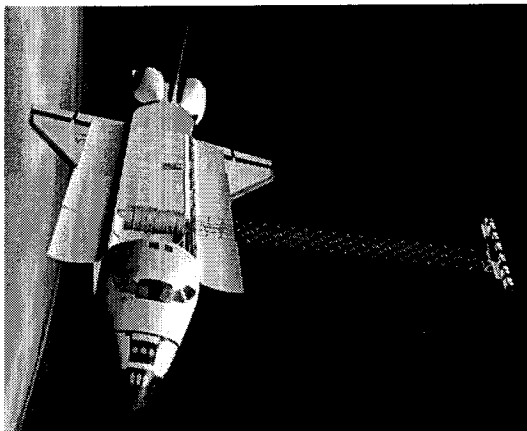


Figure 5. The 60-M Mast on SRTM

In addition to the ADAM mast, there exist many other types of off-the-shelf boom designs. These

include the collapsible booms, telescopic booms, inflatable booms, and inflatable/rigidizable booms.

2.0 Design Considerations of Space Booms and Masts

The cost for launching a space system onto its orbit is substantial and is usually a significant portion of the mission's life-cycle cost. For a typical space mission, two important drivers of launch cost are mass and launch volume. To enable the use of a smaller and usually cheaper launch vehicle, the flight system must be made low mass and compact. However, certain components, such as telescope aperture, radar antenna, solar array, sunshield, and solar sail, must have large in-orbit configurations to perform their intended functions. These components will need deployable booms to transform them from a compact launch configuration to a larger in-orbit configuration.

The design requirements for a space boom vary from one specific application to another. However, to avoid negative impacts to the launch cost, it must be lightweight and have high packaging efficiency. Additionally, a space boom usually needs to meet most, if not all, of the following requirements:

- High deployment reliability
- High post-deployment stiffness
- High post-deployment dimensional stability
- Long-term space survivability
- Design simplicity

3.0 Space Inflatable/Rigidizable Booms

The space inflatable structures have received much interest in the past few years. In particular, space inflatable/rigidizable booms provide the most impressive mass savings and packaging efficiency and can potentially meet all of the above-listed design requirements. A typical inflatable/rigidizable boom has a tubular construction. The flexible boom wall consists of three layers of membrane materials. The inner layer, called the bladder, is made of thin polyamide film and acts as the pressure barrier. The outer layer, also made of thin film, forms the enclosure for packaging and protection. The middle layer usually made of a woven material, such as graphite, Nylon, or Kevlar fabric. This middle layer is the major load-carrying element of the boom and can be coated or impregnated with selected resin that is curable in space. Once rigidized, an inflatable boom no longer requires inflation pressure to maintain its stiffness. There are currently many space rigidizable resins for inflatable booms. These

include hydro-gel, UV-curable, thermal set, and thermal plastic resin [1].

One major concern with inflatable booms rigidized by curing resins is outgassing during curing. This causes undesirable contamination and is unacceptable for missions equipped with optics. Another concern with the booms using thermal plastic and thermal set resins is that they require substantial amount of spacecraft power. These concerns have led to the re-consideration of an old rigidization approach, which was used on the ECHO balloon missions flown in the 1960s. The skin of the ECHO balloons was made of aluminum laminates, which is basically a thin layer of soft aluminum bonded in-between two constraining layers of Kapton film. An aluminum laminate becomes rigid after being stretched over its material yield point. Compared to the rigidization methods that use space curable resins, the stretched aluminum laminate approach offer the following advantages: (1) It does not require spacecraft power; (2) It has low or no outgassing; (3) Its component materials, Kapton and aluminum, have long space heritage; and (4) It takes advantage of the inflation system that is already required for inflation deployment of the boom. However, the inflatable booms rigidized by the stretched aluminum laminate approach also have the following disadvantages: (1) It requires very high inflation pressure to reach the material yield; (2) It fails by local crippling and, therefore, its buckling strength is inconsistent and hard to predict; (3) Its load-carrying capability is too low for most of space applications.

The Spring-Tape-Reinforced (STR) Aluminum Laminate Boom, developed at the Jet Propulsion Laboratory, has eliminated the disadvantages of the stretched aluminum laminate boom while retaining all of its advantages. The STR Aluminum Laminate Booms have found several important applications to radar antennas and arrays that require space booms of lengths over 5 meters. Additional details on the development and applications of the STR Aluminum Laminate Booms can be found in [2 and 3].

4.0 The “Self-deployable Spring-Strip” Boom (S³-Boom)

The basic construction of the Self-Deployable Spring Strip Boom, simply called the S³ Boom, compose of a number of axial spring tape strips connected by ring-shaped circumferential reinforcements. The axial spring strips have a curved cross-section and behave nonlinearly under axial loading. A spring strip can assume either of two bifurcation states, a stable state or a semi-stable state. When an axial spring strip is

in its stable state and maintains its curved cross section, it is capable to withstand high axial loading without buckling. When the spring strip is flattened, it is in its semi-stable state and can be easily rolled up or folded up. A large amount of energy is required to convert the axial spring strip from its stable state to semi-stable state. This energy is stowed in the rolled-up or folded-up spring strip as strain energy and is later used for self-deployment.

The function of the ring-shaped circumferential reinforcements is to connect the axial spring strips to form a boom. A circumferential reinforcement basically consists of two semicircular spring strips of a flat cross-section. There are several ways being investigated for joining the two semicircular spring strips. One is to use two flat extensions that can facilitate easy flattening of the circumferential reinforcement for stowage. Because of the flat extensions form a smooth transitions for the semicircular spring strips, a circumferential enforcement of such a design can be completely flattened without any plastic deformation of the material. We designated the S³-Booms with this type of circumferential reinforcements as the S³-FE Booms. Figure 6 shows a typical the S³-FE Booms.

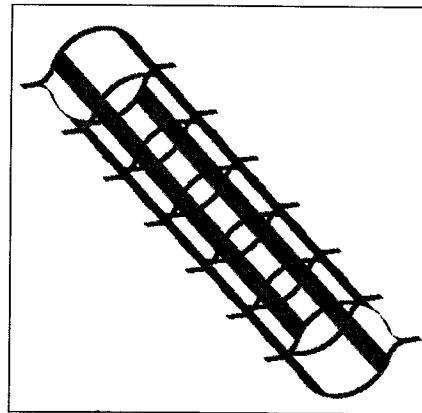


Figure 6. An S³ Boom Using Circumferential Reinforcements With Flat Extensions (the S³-FE Boom)

Because an S³-FE Boom does not experience any material yield while being flattened and stowed, it is very robust and strong. However, the flat extensions have the issue of introducing extra boom mass and volume. Also, the flat extensions can post potential safety hazards during and after the deployment of the boom. The second design approach, in which hinges, instead of flat extensions, are used to join the semicircular strips. The booms equipped with this type of circumferential reinforcements are designated as the Hinged S³-Booms. Figure 7 shows an S³-Boom. The hinges employed are made of graphite

fibers which can be bent and straighten a few times without breaking. Since these hinges are free to rotate with respect to the boom axis, a Hinged S³-Boom has considerably less load-carrying capability than an S³-FE Boom of comparable design.

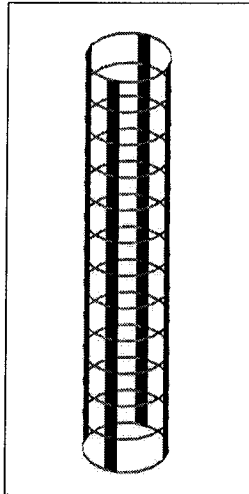


Figure 7. An S³ Boom with Hinged Circumferential Reinforcements (the Hinged S³-Boom)

The hinges in the Hinged S³ Boom can be improved by incorporating a self-locking feature. A self-locking hinge is a hinge that can rotate while the hinge is not fully opened. After the hinge is fully opened, it becomes locked in that position and can only be released manually. Because these self-locking hinges rigidly connected two semicircular spring strips after the boom is deployed, a self-locking Hinged S³ Boom is as strong and robust as the S³-FE Boom.

Additional design improvements, including new materials for the spring strips, of both the S³-FE Boom and the Hinged S³ Boom are currently being studied. We also observed that the self-deployment of an S³ Boom by sudden release of stowed energy is inherently violent and there is a need to control this process. Controllability of deployment can be obtained by several methods, including the hook-and-loop approach commonly used by other self-deployment booms. Another approach under consideration is to use a spool that has a metallic wire rolled on it. The metallic wire must be plastically deformed when it is rolled off the spool. One end of the wire is connected to the top of the self-deployable S³ Boom and the other end to the spool that is fixed at the bottom of the boom. During the self-deployment of the boom, the top of the boom is moving away from the bottom and the wire has to roll off the spool. Plastic deformation of the wire absorbs a calibrated

portion of the deployment energy and, as a result, regulates the deployment speed.

5.0 Experimental Studies of the S³-FE Boom

To facilitate laboratory testing, several S³-FE Boom samples with different composite materials have been made. We down selected one that is relatively flexible and roll it up onto a 2-inch diameter mandrel for deployment, buckling, and dynamic tests. Table 1 lists the dimensions and mass of this boom sample.

Table 1. Dimensions and Weights of the S³-FE Boom Test Sample

Overall boom diameter	5 in
Overall boom length	36 in
Width of longitudinal spring-strips	1 in
Number of longitudinal spring-strips	4
Width of circumferential spring-strips	0.25 in
Separation between circumferential spring-strips	3 in
Minimum diameter when rolled up	2 in
Weight with endcaps	0.70 lb
Weight without endcaps	0.15 lb

The sample boom was composed of three layers of carbon fiber and its areal density is estimated to be 11 oz./yd². The ratio of resin weight to total material weight is about 36%. Table 2 gives details of the composite material lay-ups.

Table 2. Composite Material lay-ups of the S³-FE Boom Test Sample

ayer #1	1 layer 2.36 oz./yd ² bidirectional graphite fiber 0°-90° fiber orientation to axial direction
ayer #2	1 layer 2.36 oz./yd ² bidirectional graphite fiber 0°-90° fiber orientation to axial direction
ayer #3	1 layer 2.36 oz./yd ² bidirectional graphite fiber 0°-90° fiber orientation to axial direction

After the sample boom was rolled up and deployed several times, buckling tests were performed. The buckling tests were conducted on a Chatillon TCM 1000-55 test stand, as shown in Figure 8. Speed was set at 0.05 inches per minute, the slowest setting. The sample boom was pin supported at each end. The maximum value of the force right before the collapse of the boom was read and recorded. This

buckling test was repeated four times. The test boom consistently failed by Euler's buckling and the results are shown in Table 3. The average buckling load of this boom is 7.6 lbs. It is believed that, some fibers might have been damaged in the first buckling test. As a result, buckling loads obtained in the subsequent tests were reduced to a consistent level of 7.5 lbs. Figure 9 shows the buckled boom.

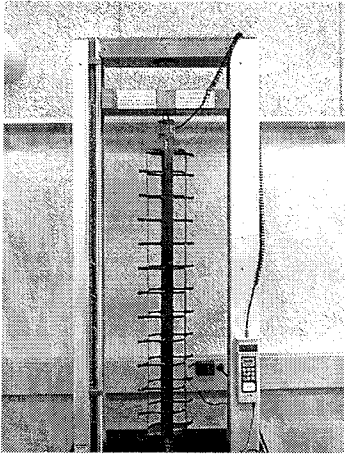


Figure 8. Buckling Test Setup (The Load Cell Is Located at The Top Of The Test Boom)

Table 3. Buckling Test Results of S³-FE Boom

Test #	Buckling loads (lbs)
Test #1	7.9
Test #2	7.5
Test #3	7.5
Test #4	7.5
Average	7.6



Figure 9. A Buckled S³-FE Boom

One Hinged S³ boom has been manufactured and tested. Another boom with rigid hinge has also been manufactured to simulate the Self-locking Hinged boom. The self-locking hinge is still under developing. Table 4 gives buckling test results of the

Hinged S³ boom and Table 5 gives buckling test results of the Self-locking Hinged S³ boom.

Table 4. Buckling Test Results of the Hinged S³ boom

Test #	Buckling loads (lbs)
Test #1	8.8
Test #2	8.4
Test #3	8.4
Test #4	8.4
Average	8.5

Table 5. Buckling Test Results of the Self-locking Hinged S³ boom

Test #	Buckling loads (lbs)
Test #1	13.2
Test #2	13.2
Test #3	12.4
Test #4	12.8
Average	12.9

By comparing Table 3 with Table 4 and 5, one can find that Self-locking Hinged S³ boom has the highest buckling load, Hinged S³ boom has the second highest buckling load and S³-FE boom has the lowest buckling load.

The S³ Boom samples were also subjected to dynamic testing on the same test stand employed in the buckling tests. Textronix 2641 Fast Fourier Analyzer was used for dynamic data acquisition. The boom was securely bolted to the top of the stand and an accelerometer was attached to the bottom to track its lateral motion. Data was collected by setting the analyzer to automatic triggering and tapping the bottom of the boom with a special mallet. Each test run consisted of five similar measurements, which were averaged by the FFT analyzer. Figure 10 is a picture of the dynamic test setup of the S³-FE boom.

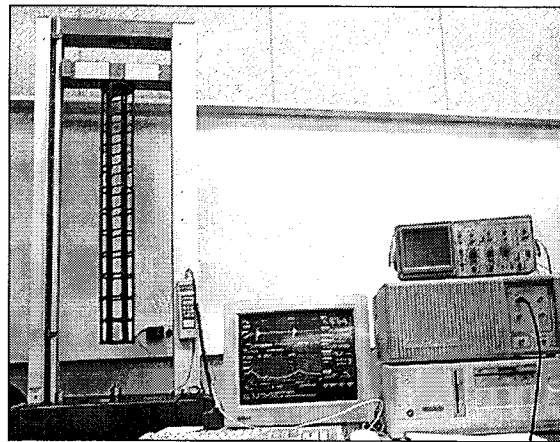


Figure 10. Dynamic Test Setup of the S³-FE boom

Figure 11 gives lateral responses both in time domain and frequency domain. The excitation was also in the lateral direction. It can be determined from this figure that the lateral resonant frequency of the sample boom is 7 Hz. Table 4 gives resonant frequencies of these three kinds of S³ boom.

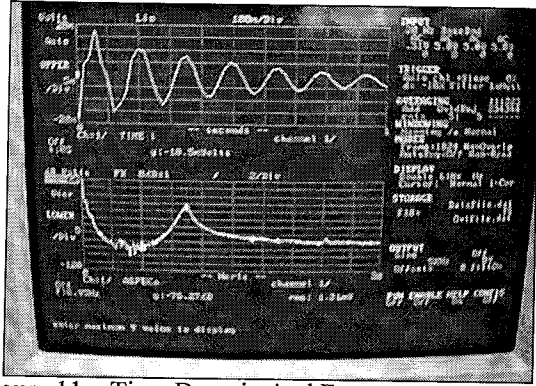


Figure 11. Time Domain And Frequency Domain Responses

Table 6. Resonant frequencies of three kinds of S³ boom.

Boom type	Resonant frequency (Hz.)
S ³ -FE boom	7.00
S ³ Hinged boom	7.15
S ³ Self-locking Hinged boom	8.35

It can be found from Table 6 that, the S³ Self-locking Hinged boom has the highest resonant frequency and the S³-FE boom has the lowest resonant frequency.

6.0 Buckling Analysis

The S³-Boom is modeled as an assembly of N_s linearly elastic shell strips and N_r circle Bernolli rings. The axial springs of the boom are modeled as longitudinal strips of a circular cylindrical shell (Fig. 12) while circumferential springs of the boom are modeled as rings (Fig. 13). The Distributed Transfer Function Method (DTFM) is used to carry out buckling analysis of the S³-Boom as shell strips and rings assembly. The DTFM is a recently developed tool for modeling and analysis of complex flexible structures. It is especially suitable and numerically efficient for plate/shell structures. In the current problem, the DTFM-based buckling analysis takes the following three steps.

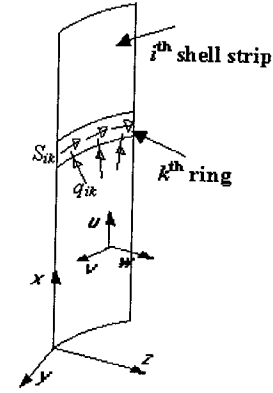


Fig. 12 the i^{th} shell strip

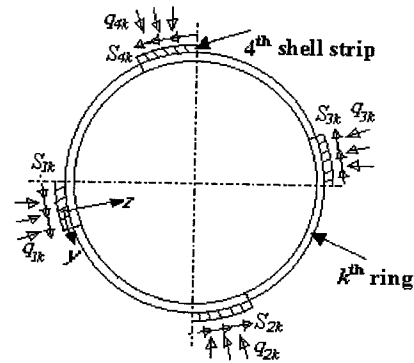


Fig. 13 the k^{th} ring

Step 1. Distributed Transfer Function of Shell Strips:

In this study, assume that there are N_s linearly elastic shell strips with length L and thickness h , and the i^{th} strip's width is from b_i^1 to b_i^2 . Donnell's shallow shell theory is applied. So, for the axial shell strips, the strain-displacement relation is given by

$$\{\varepsilon^0\} = \{\varepsilon\} + z \{\kappa\} \quad (1)$$

With the in-plane membrane strains

$$\{\varepsilon\} = \begin{pmatrix} \varepsilon_x \\ \varepsilon_y \\ \gamma_{xy} \end{pmatrix} = \begin{pmatrix} u_{,x} + \frac{1}{2} w_{,x}^2 \\ v_{,y} - \frac{w}{R} + \frac{1}{2} w_{,y}^2 \\ u_{,y} + v_{,x} + w_{,x} w_{,y} \end{pmatrix} \quad (2)$$

And the out-of-plane (bending) curvatures

$$\{\kappa\} = \begin{pmatrix} \kappa_x \\ \kappa_y \\ \kappa_{xy} \end{pmatrix} = - \begin{pmatrix} w_{,xx} \\ w_{,yy} \\ 2w_{,xy} \end{pmatrix}. \quad (3)$$

Therefore total potential energy of the shell strips is

$$\begin{aligned} \Pi = & \frac{1}{2} \int_0^L \sum_{i=1}^{Ns} \int_{b_i^1}^{b_i^2} \left(J \{\varepsilon\}^T [C] \{\varepsilon\} + D \{\kappa\}^T [C] \{\kappa\} + N_x^0 w_x^2 \right) dx dy \\ & + \sum_{k=1}^{Nr} \sum_{i=1}^{Ns} \int_{b_i^1}^{b_i^2} (q_{ik} u + S_{ik} v) \Big|_{x=x_i} dy \end{aligned} \quad (4)$$

where $J = \frac{Eh}{1-\mu^2}$, $D = \frac{Eh^3}{12(1-\mu^2)}$,

$$C = \begin{bmatrix} 1 & \mu & 0 \\ \mu & 1 & 0 \\ 0 & 0 & (1-\mu)/2 \end{bmatrix}, \quad q_{ik} \text{ and } S_{ik} \text{ are the radial}$$

and circumferential traction loads that the k^{th} ring acts on the i^{th} shell strip respectively. The membrane prebuckling force N_x^0 can be expressed by the load p as

$$N_x^0 = - \frac{p}{\sum_{i=1}^{Ns} (b_i^2 - b_i^1)} \quad (5)$$

The displacements of a shell strip element interpolated in the lateral y -direction by

$$\begin{pmatrix} u(x, y) \\ v(x, y) \\ w(x, y) \end{pmatrix} = [N(y)] \{W(x)\} \quad (6)$$

where u , v and w are the displacements of the strip in the x -, y - and z - directions (Fig. 1), respectively, the vector $\{W(x)\}$ contains the unknown displacement parameters defined along the two longitudinal sides of the strip (in x -directions), and $[N(y)]$ is the matrix of polynomial shape functions. The elements of $\{W(x)\}$ shall be called nodal line displacements. Substitution of the above displacement interpolation into the total potential energy of the shell strips (4) leads to a matrix

differential equation governing the nodal line displacements as follows:

$$\frac{\partial}{\partial x} \{\eta(x)\} = [F(p)] \{\eta(x)\} + \sum_{k=1}^{Nr} \{G(q_{ik}, S_{ik})\} \quad (7)$$

In which the state-space vector

$$\{\eta(x)\} = \begin{Bmatrix} W(x) \\ dW(x)/dx \\ d^2W(x)/dx^2 \\ d^3W(x)/dx^3 \end{Bmatrix}. \quad (8)$$

The state matrix $[F(p)]$ is a function of buckling load parameter p , the vector $\{G(q_{ik}, S_{ik})\}$ is related to the forces applied by the rings. The boundary conditions of the shell strip at its two ends (say $x = 0$ and L) can be described as

$$[M_b] \{\eta(0)\} + [N_b] \{\eta(L)\} = 0 \quad (9)$$

Where the boundary matrices $[M_b]$ and $[N_b]$ specify arbitrary boundary conditions at the strip ends.

Step 2. FEM Discretization of Rings:

The Ns shell strips are connected by the Nr ring-shaped circumferential reinforcements at $x = x_i, i = 1, \dots, Nr$ to form the S^3 -boom, here, we model them as the circle Bernolli rings. Assume the influence of the ring width be negligible, the total potential energy of the k^{th} ring is

$$\Pi = \frac{1}{2} \int_0^{2\pi R} (EA\varepsilon^T \varepsilon + EI\kappa^T \kappa) dy - \sum_{i=1}^{Ns} \int_{b_i^1}^{b_i^2} (q_{ik} u|_{x_k} + S_{ik} v^r) dy \quad (10)$$

where I is the ring moment of inertia. The strain-displacement relation is

$$\begin{aligned} \varepsilon &= \frac{\partial v^r}{\partial y} - \frac{w}{R}, \\ \kappa &= \frac{1}{R} \frac{\partial v^r}{\partial y} + \frac{\partial^2 w}{\partial y^2}, \\ v^r &= v - \bar{e} \frac{\partial w}{\partial y} \end{aligned} \quad (11)$$

where \bar{e} is the eccentricity of the centroid of the ring from the middle surface of the shell strip.

Through the general finite element discretization procedure, we have

$$[K_k]\{U_k\} = \{B(q_{ik}, S_{ik})\} \quad (12)$$

$[K_k]$ is the global stiffness matrix of the k^{th} ring, $\{U_k\}$ is the global displacement matrix of the k^{th} ring, $\{B(q_{ik}, S_{ik})\}$ is the global external loads which is relate to the applied traction with the N_s shell strips.

Step 3. Assembly of the Shell Strips and Rings:

Substituting the equation (12) into the equation (7), eliminate the applied traction forces between the shell strips and the rings, then obtain

$$\frac{\partial}{\partial x}\{\eta(x)\} = [F(p)]\{\eta(x)\} + \sum_{k=1}^{N_r} [H_k]\{\eta(x)\} \delta(x-x_k) \quad (13)$$

where $\delta(x-x_k)$ is the delta function, $[H_k]$ include the k^{th} ring state parameters. The solution of the (13) is

$$\{\eta(x)\} = \sum_{k=1}^{N_r} [Q_k(p, x)]\{\eta(x_k)\} + C_0(p, x)\{\eta(0)\} \quad (14)$$

where $[Q_k(p, x)] = e^{F(p)(x-x_k)} [H_k] u_s(x-x_k)$, $C_0(p, x) = e^{F(p)x}$, $u_s(x-x_k)$ is the unit step function. By the expression (14), we found that

$$\begin{Bmatrix} \eta(x_1) \\ \vdots \\ \eta(x_{N_r}) \end{Bmatrix} = [[I] - [Q(p)]]^{-1} \{\bar{C}(p)\} \{\eta(0)\} \quad (15)$$

where $[I]$ is the identity matrix,

$\{\bar{C}(p)\} = \{C_0(p, x_1), \dots, C_0(p, x_{N_r})\}^T$, for the matrix $[Q(p)]$, the element $Q_{ki}(p) = Q_k(p, x_i)$.

Finally by substituting (15) into (14), then utilizing the boundary condition state function (9), we obtain the following characteristic equation.

$$[K_{rs}(p)]\{\eta(0)\} = 0 \quad (16)$$

Where

$$[K_{rs}(p)] = [[\bar{M}(p)][I - [Q(p)]]^{-1} \{\bar{C}\} + [\bar{N}(p)]]$$

$$[\bar{M}(p)] = [MQ_1(p, 0) + NQ_1(p, 1), \dots, MQ_{N_r}(p, 0) + NQ_{N_r}(p, 1)]$$

$$[\bar{N}(p)] = [MC_0(p, 0) + NC_0(p, 1)]$$

So the buckling load p_{cr} of the boom is the smallest root of the characteristic equation

$$\det[K_{rs}(p)] = 0 \quad (17)$$

Once the buckling load is known, the associate mode shape can be determined as follows: first from the homogenous algebraic equation (16) determine the vector $\{\eta(0)\}$, secondly with the known p_{cr} and the known $\{\eta(0)\}$ obtain the mode shape distribution $\eta(x_1), \dots, \eta(x_{N_r})$ by Equation (15), then the configuration of each shell strips can be expressed by w .

A Matlab program has been developed and analyzed the Self-locking Hinged S^3 boom. The result is 18.3 lbs. From Table 5 we know that the experimental result is 12.9 lbs. The noticeable difference between experimental result and analysis result is believed to be caused by the different failure patterns. The analysis addressed Euler buckling while the booms tested failure by local crippling. Local crippling, controlled by material imperfections and geometrical singularities (such as bonded joints in this case) of individual booms, is difficult to predict.

7.0 Conclusions

An innovative concept of self-deployable ultra-lightweight space booms, i.e., the concept of S^3 Booms, has been proposed. Three design configurations based on this concept, the S^3 -FE Boom, Hinged S^3 Boom, and Self-locking S^3 Boom, have been developed. Proof-of-concept prototype booms have been fabricated and buckling and dynamic tests conducted on these booms. The test results showed that the Self-locking Hinged S^3 Boom has the highest resonant frequency and the buckling capability and the S^3 -FE Boom has the lowest resonant frequency and buckling capability. A

DTFM-based Euler buckling analysis procedure for the S^3 boom has also been developed. However, the obtained analysis results did not correlate well with the test results. This was due mainly to the fact that the tested booms were too short and failed by local crippling. For future development of the S^3 booms, another set of longer (much slender) boom samples will be fabricated, re-tested, and test results correlated with analytical predictions.

8.0 Acknowledgement

The work described was performed at Jet Propulsion Laboratory, California Institute of Technology under contract with the National Aeronautics and Space Administration.

9.0 References

1. Lou, M., "Development and Application of Space Inflatable Structures," Proceedings of the 22nd International Symposium on Space Technology and Science, Morioka, Japan, May 28 – June 4, 2000.
2. Yang, B., Ding, H., Fang, H., and Lou, M. "Buckling Analysis of Carpenter-Tape-Spring Reinforced Inflatable Struts," AIAA paper 2000-1725, Proceedings of the 41st AIAA/ASME/ASCE/AHS/ASC Structures, Structural Dynamics and Materials Conference, Atlanta, GA, April 3-7, 2000.
3. Lou, M., Fang, H., and Hsia, L., "A Combined Analytical and Experimental Study on Space Inflatable Booms," presented at the 2000 IEEE Aerospace Conference. Big Sky, Montana, March 18-25, 2000.
4. Yang, B., and Zhou, J., 1995, "Analysis of Ring-Stiffened Cylindrical Shells," ASME Journal of Applied Mechanics, Vol. 62, No. 4, December, pp. 1005-1014.